History information emerges in the cortex during learning

Odeya Marmor[1], Fritjof Helmchen[2,3] and Ariel Gilad[1]

1. Department of Medical Neurobiology, Faculty of Medicine, The Institute for Medical Research Israel-Canada (IMRIC), The Hebrew University of Jerusalem, Jerusalem, Israel

2. Brain Research Institute, University of Zurich, CH-8057 Zurich, Switzerland.

3. Neuroscience Center Zurich, CH-8057 Zurich, Switzerland.

Keywords: wide-field imaging. Learning. History. Barrel cortex. Posterior parietal cortex. Texture discrimination. Cortex-wide dynamics.

Corresponding author: odaya.marmor@mail.huji.ac.il, ariel.gilad@mail.huji.ac.il.

Abstract:

We learn from our experience but the underlying neuronal mechanisms incorporating past information to facilitate learning is relatively unknown. Specifically, which cortical areas encode history-related information and how is this information modulated across learning? To study the relationship between history and learning, we continuously imaged cortex-wide calcium dynamics as mice learn to use their whiskers to discriminate between two different textures. We mainly focused on comparing the same trial type with different history information, i.e., a different preceding trial. We found history information in barrel cortex (BC) during stimulus presentation. Importantly, history information in BC emerged only as the mouse learned the task. Next, we also found learning-dependent history information in rostrolateral (RL) association cortex that emerges before stimulus presentation, preceding activity in BC. History information was also found in other cortical areas and was not related to differences in body movements. Interestingly, a binary classifier could discriminate history information at the single trial level just as well as current information both in BC and RL. These findings suggest that past experience emerges in the cortex around the time of learning, starting from higher-order association area RL and propagating down (i.e., top-down projection) to lower-order BC where it can be integrated with incoming sensory information. This integration between the past and present may facilitate learning.

Introduction:

Learning is a process of acquiring new knowledge required for appropriate behavior and is highly dependent on our previous experience. Our brain integrates incoming sensory information with history information of previous stimuli to form a knowledgeable association of the current stimulus. Despite the strong link between history and learning, the underlying cortex-wide dynamics are relatively unknown, partially because most previous studies separately focus either on learning or history(Hattori et al., 2019). Learning-related neuronal dynamics are broadly observed across the whole cortex, including primary sensory or motor areas(Blake et al., 2002; Chen et al., 2015; Gilad and Helmchen, 2020; Jurjut et al., 2017; Komiyama et al., 2010; Li et al., 2008; Poort et al., 2015; Wiest et al., 2010; Xu et al., 2014; Yan et al., 2014), higher-order association areas(Driscoll et al., 2017b; Gilad and Helmchen, 2020) and prefrontal cortex(le Merre et al., 2018; Pasupathy and Miller, 2005). But do these areas that participate in the learning process also carry history information?

Encoding of history information has been reported mainly in higher order cortical areas such as the posterior parietal cortex (PPC)(Akrami et al., 2018; Harvey et al., 2012; Hwang et al., 2017; Morcos and Harvey, 2016; Benjamin B Scott et al., 2017; Suzuki et al., 2022) , retrosplenial cortex(Hattori et al., 2019; Vann et al., 2009) and prefrontal cortex (Banerjee et al., 2020; Johnson et al., 2016; Kawai et al., 2015; Benjamin B. Scott et al., 2017; Sul et al., 2010; Tsutsui et al., 2016) , but also to a smaller extent in lower-order primary sensory areas such as BC(Banerjee et al., 2020; Chéreau et al., 2020; Rodgers et al., 2021). There is still a debate on which areas link history information with the learning process. Another important aspect of the history-learning relationship is the temporal aspect that enables integration of past information with present sensory information. For example, does history information emerges in cortex before present information arrives or do both past and present information maybe emerge simultaneously in a certain cortical area? From the temporal aspect, optogenetic silencing of PPC area during the inter-trial interval affected performance, highlighting that higher-order cortical areas may maintain history information before the incoming current stimulus(Akrami et al., 2018; Hwang et al., 2017).

To study the history-learning relationship, we use wide-field cortical imaging of mice learning to discriminate between two textures and focus on the cortex-wide

dynamics of history information. In a previous study using the same dataset, we showed that in mice learning a whisker-based texture discrimination task, the activity in task-related areas (e.g., barrel cortex – BC and rostrolateral association cortex – RL) increases as they become experts(Gilad and Helmchen, 2020). RL is part of the PPC and is located within the cluster of higher-order association areas surrounding V1. RL plays pivotal roles in cross-modal sensory integration, learning and history, but the relationship between history and learning in RL is unknown (Akrami et al., 2018; Driscoll et al., 2017a; Hattori et al., 2019; Hwang et al., 2017; Khodagholy et al., n.d.; Marcos and Harvey, 2016; Save and Poucet, 2009). Here, by classifying trials according to the preceding trial, we now demonstrate the emergence of history information as the mouse gains expertise. Specifically, history information emerges in RL, just before the stimulus presentation during the trials, and then is transferred to BC during the texture touch period, which may aid in learning the rewarded stimulus.

Results:

In this study we investigate history-dependent dynamics across the whole dorsal cortex and its emergence during learning in transgenic mice expressing a calcium indicator (GCaMP6f) in L2/3 excitatory neurons (n=7 mice). This dataset is identical to the one published in Gilad and Helmchen(Gilad and Helmchen, 2020) where we focused only on learning dynamics. Using wide-field calcium imaging through the intact skull (Gallero-Salas et al., 2021; Gilad et al., 2018b; Gilad and Helmchen, 2020; Vanni and Murphy, 2014), we chronically measured large-scale neocortical L2/3 activity in the contralateral hemisphere as mice learned a go/no-go whisker-dependent texture discrimination task (Gilad and Helmchen, 2020). Whisker movements and body movements were video monitored and synchronized to the calcium imaging data (Methods). To delineate areas in the dorsal cortex, we functionally mapped sensory areas for each mouse during anesthesia (see Methods). Based on these maps (and skull coordinates) we registered all images to the 2D top-view Allen reference atlas(Oh et al., 2014) and defined 25 areas of interest, further divided into four groups (Fig. 1c;(Gilad and Helmchen, 2020)).

Mice were trained on a head-fixed, whisker-based go/no-go texture discrimination task (Chen et al., 2013; Gilad and Helmchen, 2020)(Fig. 1a; Methods). Each trial started with an auditory cue (stimulus cue), signaling the approach of either two types of sandpapers (grit size P100: rough texture; P1200: smooth texture; 3M) to the mouse's whiskers as 'go' or 'no-go' textures. The texture stayed in touch with the whiskers for 2 s, and then it was moved out after which an additional auditory cue (response cue) signaled the start of a 2-s response period (Fig. 1b) followed by a 6-s break until the next trial auditory cue. Five mice were trained to lick for the P100 and two mice were trained to lick for the P1200 texture. Mice were rewarded in 'Hit' trials for correctly licking after the go texture and punished with white noise for incorrectly licking for the no-go texture ('false alarm' trials, FA). Mice were neither rewarded nor punished when they withheld licking for the go and no-go textures ('Miss' and 'correct-rejection', CR, trials, respectively). We defined two time windows within the trial structure: the 'pre-period' when the texture approaches the whiskers (−1 to −0.6 s relative to the texture stop; mainly before the first whisker-texture touch); and the 'stim-period' during texture touch (−0.2 to 0.2 s relative to texture stop; Fig. 1b).

The performance of all mice increased with training (5–11 days; ~500 trials/day) and eventually reached high discrimination levels (quantified by d-prime; d'; Fig. s1; refs. (Gilad et al., 2018a); Methods). We defined the 'learning threshold' of reaching expert level for each mouse by crossing the inflection point of the sigmoid fit for the learning curve (in units of 'trial number'; Fig. 1e, Fig. s1). The fastest learning mouse reached threshold in slightly less than thousand trials whereas mouse #4 took substantially longer (Fig. s1). In addition, we defined a naïve (1st day of recording), learning (day of crossing the learning threshold; 2nd or 3rd day) and expert (last recording day) phases for each mouse. All mice, after gaining expertise, showed strong activation in the Barrel cortex (Fig 1. d, upper panel). This activation was during stimulus representation, stronger in Hit trials compared to CR trials (Fig. 1d, lower panel), not dependent on the texture type (i.e. if the hit was p100 or p1200).

Here, we focus on the history content for each trial type. We sub-grouped all the Hit trials (i.e., the current trial type) based on the previous trial type: CR ("CR-Hit"; n=423±74, mean±SEM), Hit ("Hit-Hit"; n=585±42), FA ("FA-Hit"; n=217±24) or Miss ("Miss-Hit"; n=55±24; Fig.1f, g). "Miss-Hit" were not analyzed due to a small number of trials. Our main analysis will compare "CR-Hit" (orange) and "Hit-Hit" (blue) trial pairs, since they are present in large numbers during all phases in each mouse separately (Fig. 1g; But see Fig. s3 for a comparison of other trial pairs). We emphasize that in this comparison, the current trial type is identical (i.e., Hit) whereas only the pervious trial (i.e., the history, CR or Hit) differed, therefore eliminating activity differences due to the current stimulus.

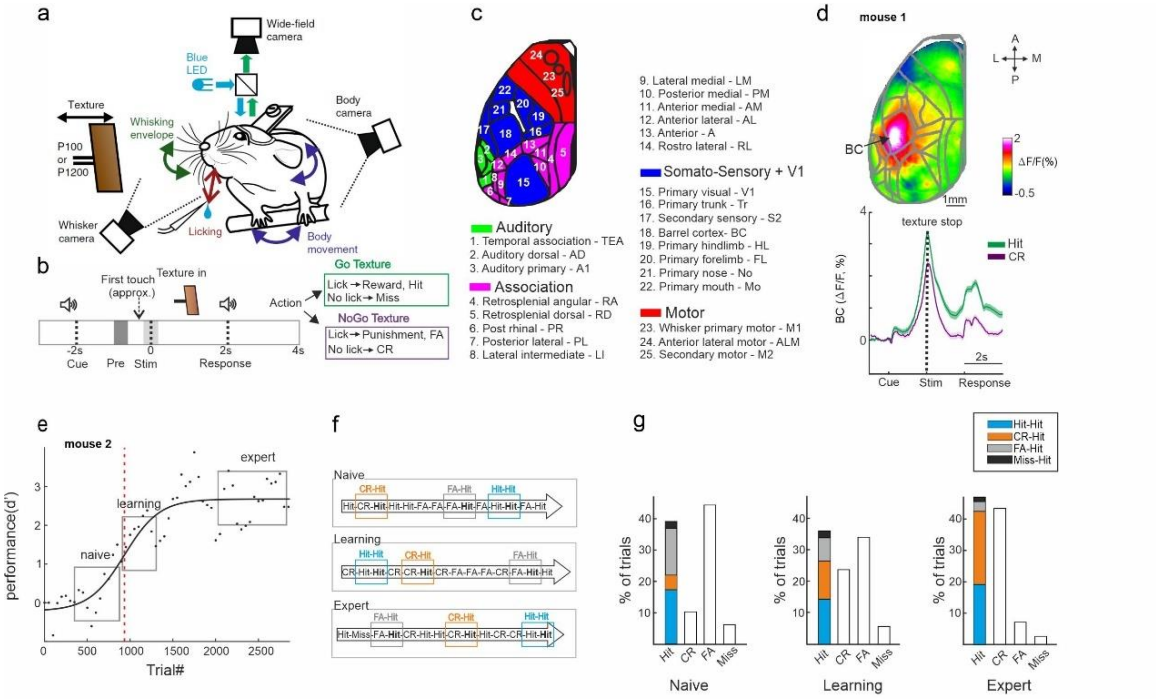

Figure 1. Trial types based on history

a. Behavioral setup for head-fixed texture discrimination with simultaneous wide-field calcium imaging and video monitoring of whisker motion and body movement. **b**. Trial structure and possible trial outcomes. pre- and stim-periods are marked in gray and light gray colors, respectively. **c.** 25 cortical areas used in this study grouped into auditory areas (green), association areas (pink), somatosensory + V1 areas (blue), and motor areas (red) **d.** *Top:* Example mean activation map (averaged during the stim period) for the Hit condition. BC – barrel cortex. Color denotes normalized fluorescence. Bottom: Time course of activity in BC for Hit (green) and CR (purple). Error bars are mean±SEM across trials (n=376 and 333 for Hit and CR respectively). **e.** Example of a learning curve (d' as a function of trial number) of one mouse, fitted with a sigmoid function (solid black line). Red dashed vertical line indicates the learning threshold. gray rectangles mark the naive, learning and expert phases. **f.** Schematic diagram of the different trial types for a Hit trial preceded by a different trial (i.e., history): Hit-Hit (blue), CR-Hit (orange) and FA-Hit (gray). **g.** Probability of the different trial types along with the distribution of history for the Hit trial during the naïve, learning and expert phases (averaged across 7 mice).

History information in BC emerges during learning

First, we focused on history-dependent information in BC, specifically during the stim-period. BC displayed higher activity during CR-Hit compared to Hit-Hit only during learning and expert phases, but not during the naïve period (Fig. 2a, Fig. s2). This difference was significant during the stim-period in learning and expert phases across

mice (Fig. 2b; signed rank test, $p<0.05$). To check whether this effect is not due to difference in body or whisker movements between the two pair types, we analyzed body movements by calculating (1 - frame-to-frame correlation) in mouth, forelimb and hindlimb areas and computed whisker envelope as a function of time (see Methods). Both body movements and whisker envelope were similar between CR-Hit and Hit-Hit pairs (Fig. 2c) and there was no significant difference across mice during the stim-period for neither naïve, learning or expert phases (Fig. 2d $p>0.05$; Signed rank test) nor during the pre-period ($p>0.05$, signed rank test, data not shown). This result, along with the fact that the current trial type in both conditions is identical, strongly indicates the presence of history information in BC.

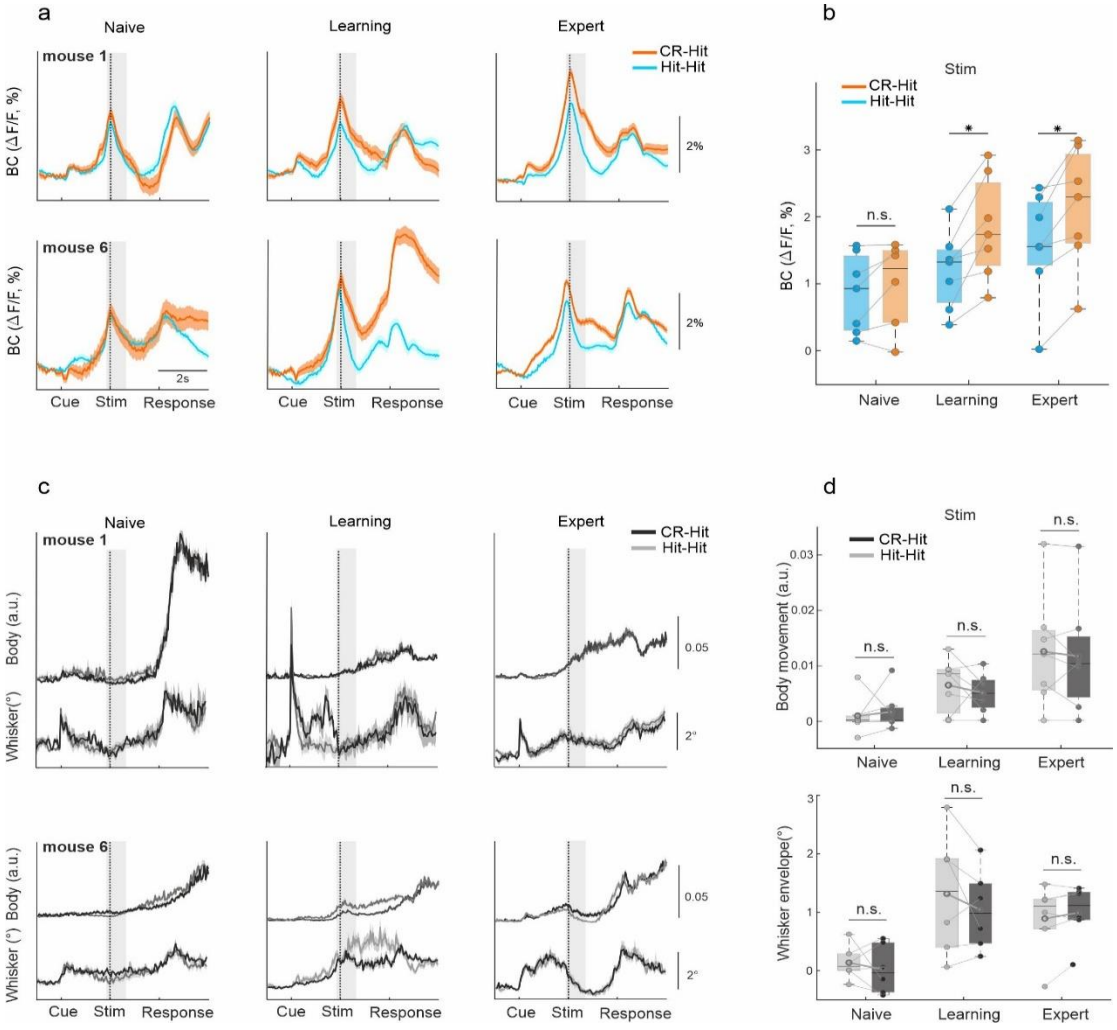

Figure 2. History information in BC

a. Example of average BC response of Hit-Hit (blue) and CR-Hit (orange) from 2 mice (upper and lower row) in the naïve, learning and expert phases. Shaded bar depicts the stim period. Shadows are mean±SEM across trials (mouse 1: n=86/66, 90/70 and 166/173 Hit-Hit/CR-Hit for naïve, learning and expert phases respectively. mouse 6: n=94/80, 86/121 and 99/135) **b.** Grand average of BC activity during the stim period (-0.2:0.6ms) for the naïve, learning and expert phases. Boxes indicate quartiles at 25/75th percentile across mice (n=7). **c.** Same as **a** but for body and whisker movements in the Hit-Hit (light gray) and CR-Hit (dark gray) trials. **d.** Same as **b** but for body (top) and whisker (bottom) movements. *p < 0.05; n.s. not significant; Wilcoxon signed-rank test.

We next quantified the emergence of history information with regard to the different time scales, the trial structure (within seconds) or the learning profile (across days). We first show 2D activity plots in BC for each trial pair (i.e., CR-Hit and Hit-Hit; showing activity of only the Hit trial), where trial time is plotted on the x-axis and trial number across learning time on the y-axis (Fig. 3a; 100-trial bins regardless of trial pair). Both

158 trial pairs display an increase in activity during the stim-period shortly after passing the
159 learning threshold. We defined a history modulation index as the difference in activity
160 for BC between the two pair types (Hit-CR minus Hit-Hit). History modulation increased
161 around the stim-period only in learning and expert phases but not in the naïve case
162 (Fig 3b, c). A significant history modulation was defined as values exceeding mean±2SD
163 of a trial-shuffled sample distribution (n=1000 iterations) and was performed for each
164 mouse separately (Fig. 3b). The onset of the history modulation was defined as the first
165 time frame reaching significant values (red arrows in Fig. 3b) and was found in BC to
166 be during the stim-period (Fig. 3d; 0.05±0.32s, -0.1±0.27s 1s, median±SEM relative to
167 texture stop in learning and expert phases respectively). We note that in the expert
168 phase there is also a small peak exceeding the significance around the cue, indicating
169 history information in BC may be present to some extent before stimulus presentation.
170 Next, we quantified the history modulation in BC during the stim period as a function
171 of the learning time course. History modulation in BC had the steepest increase after
172 each mouse crossed its learning threshold (Fig. 3e, f). The onset of the history
173 modulation was defined as the first trial bin exceeding the trial-shuffled sample
174 distribution and was found to occur shortly after the learning threshold, highly
175 correlated with the learning threshold indicating strong relationship between history
176 emergence and learning of each individual mouse (Fig. 3g, h; 500±83 trials,
177 median±SEM, r=0.97 $p<0.001$, spearman correlation). Note that our onset
178 measurement is relatively strict and an increase in history information can be observed
179 shortly (i.e., tens of trials) after crossing the learning threshold (Fig. 3d).

180 We expanded our history analysis also for the pair types other than CR-Hit and Hit-Hit.
181 For sufficient trial numbers, we focused on the learning phase. First, we compare FA-
182 Hit to Hit-Hit and CR-Hit, i.e., the same current trial type but preceded by an error trial
183 (FA). Response in BC for FA-Hit was similar to Hit-Hit and significantly lower compared
184 to CR-Hit (Fig. s3; $p<0.05$ signed rank test). This result highlights that specifically a
185 correct rejection (CR), rather than the stimulus (i.e., texture) type, has a strong history
186 effect. Next, we compared FA-CR, Hit-CR and CR-CR, i.e., similar to the previous
187 comparison differing only in the current trial type (CR instead of Hit). There was no
188 significant difference between the different pairs, indicating that the current trial type,
189 i.e., Hit in this case, has a strong effect along with the history of the CR (Fig. s3; $p>0.05$,
190 signed rank test). A comparison of FA-FA, Hit-FA and CR-FA did not show a significant
191 difference (Fig. s3; $p>0.05$, signed rank test). In general, a preceding CR trial resulted in

192 higher activation independent of the current trial type (i.e., Hit, CR or FA; not significant
193 for CR and FA), indicating that history information is present at the current time
194 independently of incoming sensory information (Fig. s3; Compare orange bars to the
195 blue bars). In conclusion, we found that the CR-Hit pair displayed a specific
196 enhancement in BC that is related both to the preceding and current trial type (see
197 discussion).
198
199 Next, we expanded our analysis to the whole dorsal cortex during the stim
200 period. Mean activation maps for both CR-Hit and Hit-Hit pairs (i.e., Activity for the
201 current Hit trial whereas only the preceding trial was different) during the stim period
202 displayed a pronounced activation patch in BC during naïve, learning and expert phases
203 (Fig. 4a). BC activity was higher in CR-Hit compared to Hit-Hit especially during learning
204 and expert phases. The grand average activity for all 25 cortical areas highlights history-
205 dependent information that emerges during learning (Fig. 4b). We note that other
206 areas, e.g., different association areas, also encoded history-dependent information
207 especially during learning and expert phases. Taken together, these results indicate
208 that BC encodes history-dependent information that emerges during the stim period
209 and just after learning. These results gave us the motivation to examine history-
210 dependent information at time periods before texture touch.

211

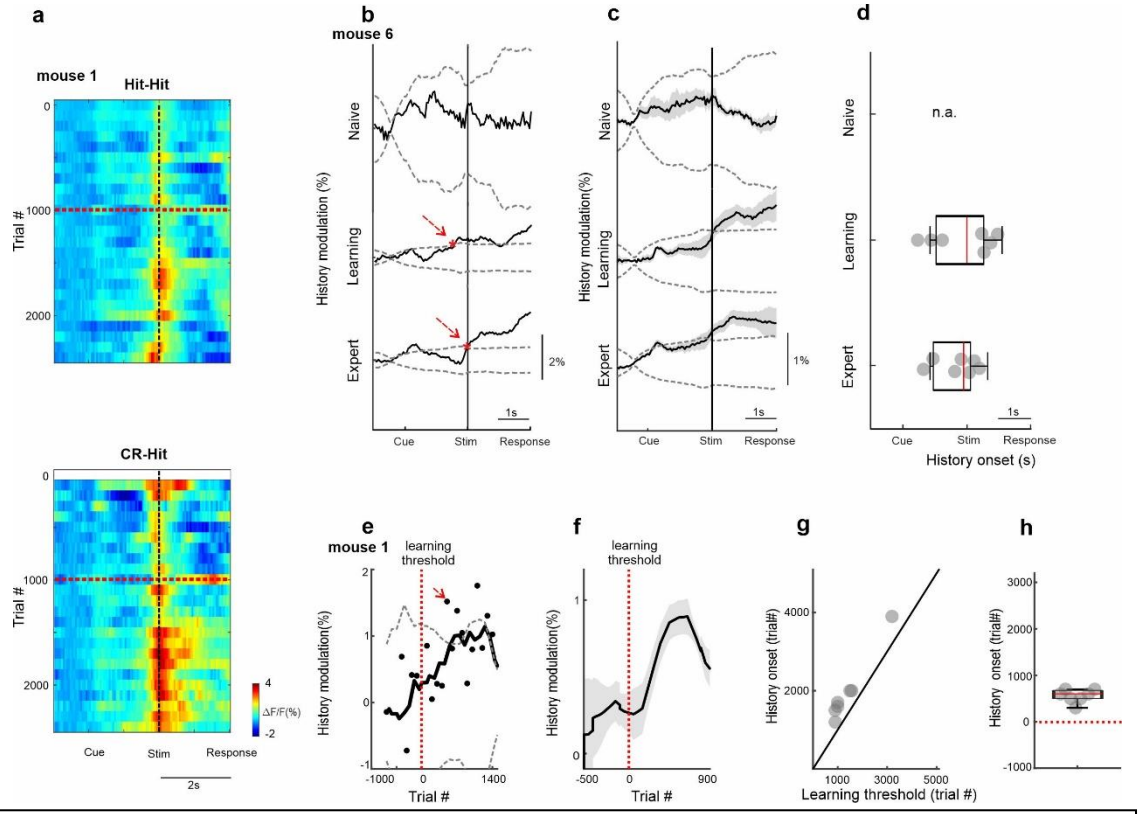

Figure 3. Temporal dynamics of history information in BC

a. 2D plot of BC responses for Hit-Hit (top) and CR-Hit (bottom; trial structure on x-axis; Trial number across learning (in bins of 100 trials) on the y-axis. Red horizontal dashed line indicates learning threshold. Black dashed vertical line indicates the time of texture stop. **b**. Example from one mouse of the history modulation (activity in CR-Hit minus activity in Hit-Hit) in BC along the trial structure in the naïve, learning and expert phases. Dashed gray line is the mean ± 2 SD of the trial-shuffled data (n=1000 iterations). The first-time frame crossing the shuffle data is defined as the onset and is marked in red. **c**. Mean history modulation in BC along trial time. Shadows depict mean±SEM across mice (n=7). **d**. Median onset of history modulation. Boxes indicate quartiles at 25/75th percentile across mice (n=7). **e**. Example from one mouse of the history modulation along learning dimension. Dashed gray line is the mean ± 2 SD of the trial-shuffled data (n=1000 iterations). The first-time frame crossing the shuffle data is defined as the onset for learning and is marked in red. The vertical red dashed line (trial 0) marks the learning threshold. **f.** Mean history modulation in BC along the learning profile aligned to the learning threshold of each mouse (time 0). Shadows depict mean±SEM across mice (n=7). **g**. Onset of the history modulation for learning as a function of the learning threshold. Each point is one mouse (n=7). **h**. Median onset of history modulation relative to the learning threshold. Boxes indicate quartiles at 25/75th percentile across mice (n=7).

212

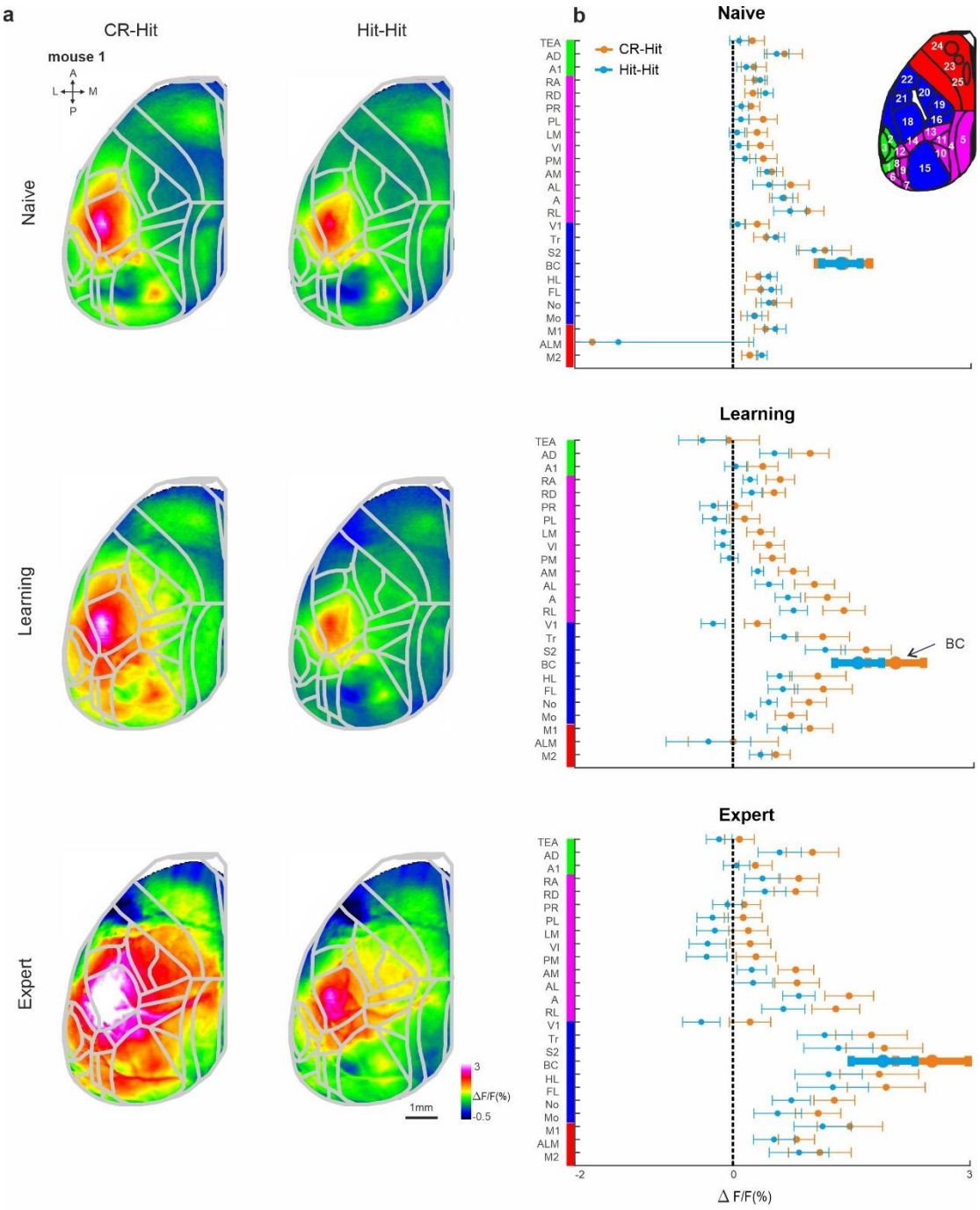

Figure 4. Cortex-wide history modulation during the stim period.

a. Mean activity maps averaged within the stim period (-0.2 – 0 seconds relative to texture stop) of CR-Hit (left) Hit-Hit (right) during the naïve (top), learning (middle), expert (bottom) phases. Color bar denotes normalized fluorescence (ΔF/F). 2D top-view atlas is superimposed in gray. **b**. Grand average neuronal activity during the stim period (-0.2:0.2s) for Hit-Hit (blue) and CR-Hit (orange) in all 25 areas for the naïve (top), learning (middle) and expert (bottom) phases. Error bars depict mean±SEM across mice (n=7).

213

History information in RL before sensation

We next focused our analysis on the pre-period, just before texture touch (-1 to -0.6 sec before texture stop). Mean activity maps during the pre-period highlight activity in association area rostrolateral (RL) that is present for both CR-Hit and Hit-Hit pairs during the naïve, learning and expert phases (Fig. 5a;(Gilad and Helmchen, 2020)) RL pre-period activity is higher in CR-Hit compared to Hit-Hit mostly during learning and expert phases. In addition, higher RL activity in CR-Hit pair starts even before the pre-period, indicating that history-information is not directly related on the current stimulus (Fig. 5b). The grand average of all 25 cortical areas, highlights the emergence of history-dependent information emerging during learning, especially in RL, but also in other association and sensory areas (Fig. 5c).

RL activity was significantly higher in CR-Hit compared to Hit-Hit trials in the pre- period during the expert phase (Fig. s4; signed rank test, $p<0.05$, similar trend for the learning phase but insignificant; not significant for the naïve phase). The onset of history modulation within the trial structure (as in Fig. 3d) was earlier in RL compared to BC in both learning (-0.15±0.32s and 0.05±0.32s, median±SEM in RL and BC respectively) and expert phases (-0.75±0.2s and -0.1±0.27s, median±SEM in RL and BC respectively) but not significantly different ($p>0.05$, signed rank test). The onset for the history modulation with relation to the learning profile in RL (similar to Fig. 3h; During the pre-period) was also earlier than BC, but not significantly different (200±162 trials after crossing threshold compared to 500±83 in BC; median±SEM, $p>0.05$ singed rank test). Taken together, these results indicate that as mice gain expertise, RL encodes history information before the next stimulus occurs, which may inform through its projections to BC where history information then could be integrated with information of the current incoming texture.

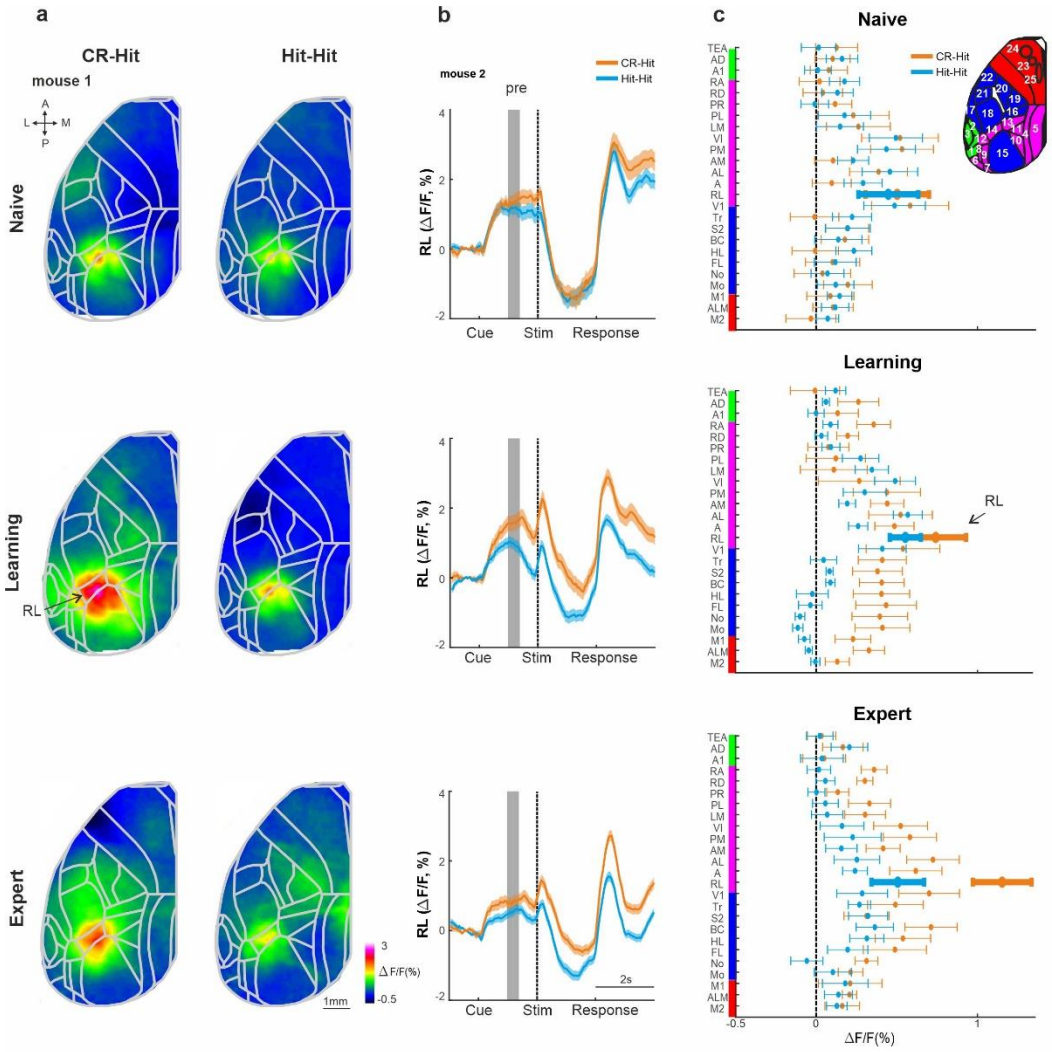

Figure 5. History information in RL before stimulus presentation.

a. Mean activity maps averaged within the pre-period (-1 – -0.8 seconds relative to texture stop) of CR-Hit (left) Hit-Hit (right) during the naïve (top), learning (middle), expert (bottom) phases. Color bar denotes normalized fluorescence (ΔF/F). 2D top-view atlas is superimposed in gray. **b.** Example from one mouse of average RL response of Hit-Hit (blue) and CR-Hit (orange) in the naïve (top), learning (middle) and expert (bottom) phases. Shaded gray bar depicts the pre-period (-1– -0.6). Shadows are mean±SEM across trials (n=51/54, 92/78 and 168/173 Hit-Hit/CR-Hit for naïve, learning and expert phases respectively) **c.** Grand average neuronal activity during the pre-period (-1 – -0.6) for Hit-Hit (blue) and CR-Hit (orange) in all 25 areas for the naïve (top), learning (middle) and expert (bottom) phases. Error bars depict mean±SEM across mice (n=7).

Past versus present discrimination power in BC and RL

How well can BC and RL activity discriminate at the single trial level history information compared to the information of the current stimulus? To do this, we computed the receiver operating characteristics (ROC) analysis between specific trial types(Gilad et al., 2020, 2013) , along with the area under the curve (AUC) quantifying the discrimination power at the single trial level (Methods). We calculated the AUC between two types of trials (Fig. 6a): 1) Activity between CR-Hit and Hit-Hit pairs based on the activity during the Hit trial. This is defined as 'history-AUC' since only the previous trial is different. 2) Activity between the current Hit and CR trials. This is defined as the 'Current-AUC' because the current trial types are different (both in terms of stimulus type and action). Both history-AUC and current-AUC are calculated for BC and RL for each time frame along the trial structure and for naïve, learning and expert phases. Intuitively, one would assume that the current-AUC will display higher discrimination power compared to the history-AUC because the latter AUC measure compares the same current trial type which should be harder to discriminate. Interestingly, during the expert phase, history-

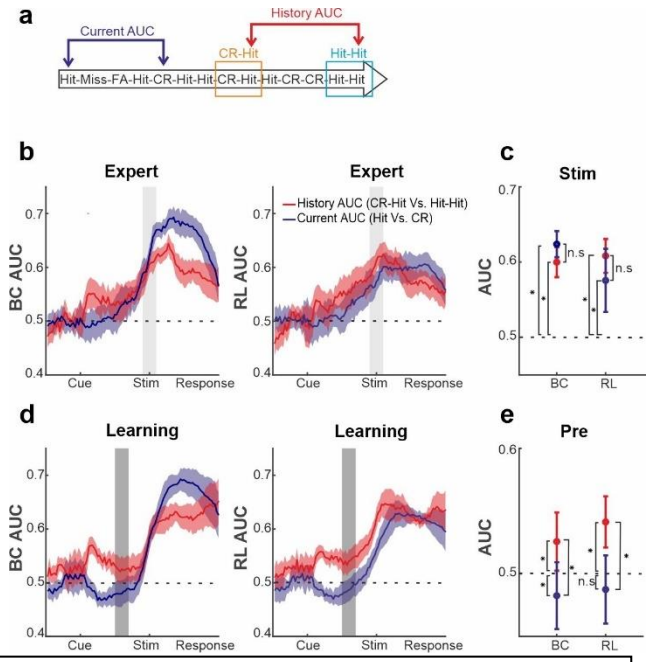

Fig. 6. History and current information are equally discriminative at the single trial level

a. Schematic diagram for the two types of area under the curve (AUC) measures (derived from a ROC analysis): history-AUC between the Hit responses for Hit-Hit and CR-Hit trial types. Current-AUC between Hit and CR trial types regardless of their history. **b.** Grand average of the history (red) and current (blue) AUC measures in BC (left) and RL (right) along the trial structure during the expert phase. Shadows depict mean±SEM across mice (n=7). Values significantly differ from chance (0.5) in history-AUC ($p<0.05$, 2 tail ttest, for both BC and RL). **c.** Grand average of history and current-AUC measures during the stim period in the expert phase. Error bars indicate mean±SEM across mice(n=7). **d.** Same as in a but for the learning phase. Error bars as in a, values significantly differ from chance (0.5) for history-AUC ($p<0.05$, 2 tail ttest, for both BC and RL), but not for the current-AUC in RL. **e.** same as in c, but for the pre-period during the learning phase. *$p < 0.05$; n.s. not significant; Wilcoxon signed-rank test.

AUC in both BC and RL has a discrimination power in the stim period that is not significantly different than that of the current-AUC (Fig. 6b, c; $p>0.05$; singed rank test). In other words, we found that BC and RL discriminate past stimuli just as well as the current stimuli. In addition, during the learning phase, RL and to some extent BC, display a significantly higher history-AUC compared to the current-AUC, specifically in the pre-period (Fig. 6d, e; $p<0.05$; Singed rank test). This indicates that history information is discriminative at the single trial level before stimulus onset. Taken together, we find that BC and RL can encode the past just as well as the present.

Discussion:

History information is trial-type specific

We have identified cortex wide encoding of history information that emerges as mice learn to discriminate between two textures. History information was not dependent on the current stimulus and emerged in RL association area before texture touch. Our results indicate that a previous CR trial will lead to higher activity in BC and RL compared to a previous Hit trial. This difference is probably not due to pure sensory differences in the previous trial since the effect was not present after FA trials (sup Fig. s3, left panel). In addition, mice trained to lick the P1200 texture displayed a similar bias to the CR-Hit, further indicating that these differences are not purely sensory related. Moreover, this difference is probably not related to the previous motor action (e.g., either lick or no-lick). During the current trial, body and whisker movements were not significantly different, emphasizing that there are no motor-related differences based on the previous trial (Fig. 2c, d). The fact that these differences emerged only after learning implies that these differences are not purely sensory or motor related but rather reflect internal history-related information. It may be that in a go/no-go discrimination task the mouse mainly learns not to lick for the no-go texture (i.e., CR) making the information of a CR trials more pronounced relatively to a Hit trials. Another possibility is that a previous CR will cause a pronounced anticipatory state for the incoming texture, leading to enhanced cortical activity. Again, we did not find any consistent differences in motor movements based on the previous trials making this possibility less likely. In summary, our results indicate that history-dependent information emerges internally in cortex as mice learn to discriminate between two stimuli.

History information emerges in RL and transferred to BC

BC is considered a lower-order sensory area but encodes not only lower-order stimulus features(Chen et al., 2013; Estebanez et al., 2012; Garion et al., 2014; Safaai et al., 2013) but also higher-order information such as choice and reward value(Chéreau et al., 2020; Rodgers et al., 2021; Zuo and Diamond, 2019). We additionally found that BC carries history information during the sensation period which is related to the previous trial several seconds back. The presence of history information in lower-order areas such as BC is interesting by itself, but also raises the question of where is its origin. Interestingly, we show that history information emerges in RL before texture touch implying that RL may transfer history information in a top-down manner to BC for optimal sensory integration.

The presence of history information in RL before the sensation period implies that RL may play a crucial role in linking past experience to ongoing sensory integration. RL is the lateral part of PPC adjacent to BC, within the cluster of higher-order association areas surrounding V1 (Hovde et al., 2018; Lyamzin and Benucci, 2019). Previous studies showed that history information of choice-outcome is encoded by PPC neurons(Harvey et al., 2012; Hwang et al., 2017; Marcos and Harvey, 2016; Pho et al., 2018), as well as history of sensory information(Akrami et al., 2018). Silencing the PPC specifically during the inter-trial interval affected the behavioral performance of rats (Akrami et al., 2018; Hwang et al., 2017), whereas silencing during the stimulus presentation did not affected performance. The PPC is also reciprocally connected to hippocampus via entorhinal and retrosplenial cortices (Save and Poucet, 2009; Whitlock et al., 2008) and to basolateral amygdala via the anterior cingulate cortex (Suzuki et al., 2022), giving fast access to the different memory hubs. Khodagholy et al.(Khodagholy et al., 2017) showed coupling of PPC and hippocampal ripples that strengthen in non-REM sleep after rats learned a spatial exploration task, further indicating that RL may relay history information from subcortical memory hubs to cortex.

The fact that history information emerges only after learning, implies that it encodes a subjective value or association of a certain past stimulus. It may be that only once the value of a certain stimulus has been established, e.g., by strengthening indirect connections between basolateral amygdala (that has a role in associative memory) and RL, history information can aid in efficiently encoding the incoming stimulus. In light of this discussion, we suggest that the consolidation of a certain

association (in our case a CR), induces long-term synaptic plasticity of top-down projections from higher-order association area (e.g., RL) to a lower-order sensory area (e.g., BC). This projection-specific potentiation may better recruit sensory cortex in the context of the immediate previous history.

Mechanisms for integrating past and present

The wide-field signal measured in our study reports bulk population activity specifically in L2/3 excitatory cells. Are neuronal populations encoding past and present information in the BC overlapping or distinct? On one side, it could be that the same cell in BC encodes both the current stimulus and additionally receives top-down input from RL carrying the past stimulus identity. This additional top down information may amplify sensory integration and optimize discrimination of the current stimulus. On the other side, previous studies that measured single cell activity in the BC showed that single cells tend to respond to one information type, (Chéreau et al., 2020; Estebanez et al., 2012; Rodgers et al., 2021). In this case, we hypothesize that different populations in BC encode current and history information, which leads to a larger fraction of neurons in BC that are active for the CR-Hit pair. A larger number of active neurons in BC may facilitate sensorimotor integration involving downstream areas such as the motor cortex, further resulting in gaining an expert level (Zuo and Diamond, 2019).

It is probable that both history and learning involve other circuit elements such as deep cortical layers (Pasupathy and Miller, 2005; Roelfsema and Holtmaat, 2018; Vecchia et al., 2020), inhibitory subtypes, other pathways (Lacefield et al., 2019; Mohan et al., 2022; Musall et al., n.d.; Petreanu et al., 2012; Williams and Holtmaat, 2019),and subcortical areas (Fu et al., n.d.; Garrett et al., 2020; Pasupathy and Miller, 2005; Pfeffer et al., 2013). Future work may aim to dissect specific subpopulations that carry history information using similar behavioral tasks, e.g., imaging of cortex-wide layer 5 dynamics. Layer 5 neurons may be ideal in integrating past information arriving onto the apical dendrites in layer 1[54] with incoming information arriving from the thalamus. In addition, similar tasks with reward after CR trials, or tasks that better differentiate between choice and outcome (decision tasks, giving different probabilities of outcome to each choice), or tasks with a dynamic inter-trial interval may shed light on the meaning of this history-learning effect. In summary, our results

imply that as we learn, the cortex learns to better integrate past and present information resulting in expert performance.

Acknowledgements:

This project has received funding from the European Union's Horizon 2020 research and innovation program under the Marie Skłodowska-Curie grant agreement No 659719 (A.G.). This work was supported by grants from Hebrew University of Jerusalem (Start-up grant; A.G.) and the Swiss National Science Foundation (SNSF) (31003A-149858 and 310030B_170269; F.H.).

declaration of interests:

The authors declare no competing interests.

Data and code availability:

The data and code that support the findings of this study are available at https://osf.io/hkvc5.

Author contributions: A.G. and F.H. designed the experiments. A.G. conducted the experiments. A.G. and O.M. performed data analysis. A.G. and O.M. wrote the manuscript with comments from F.H.

Star methods:

Animals and surgical procedures:

Methods were carried out according to the guidelines of the Veterinary Office of Switzerland and following approval by the Cantonal Veterinary Office in Zurich. A total of 7 adult male mice (1-4 months old) were used in this study. These mice were triple transgenic Rasgrf2-2A-dCre; CamK2a-tTA;TITL-GCaMP6f animals, expressing GCaMP6f in excitatory neocortical layer 2/3 neurons (Gilad and Helmchen, 2020). The dataset used here is identical to our previous study (Gilad and Helmchen, 2020), but here we have applied a completely novel history analysis. To generate triple transgenic animals, double transgenic mice carrying CamK2a-Tta62 and TITL-GCaMP6f63 were crossed with a Rasgrf2-2A-dCre line (64; individual lines are available from The Jackson Laboratory as JAX# 016198, JAX#024103, and JAX# 22864, respectively). The Rasgrf2-2A-dCre;CamK2a-tTA;TITL-GCaMP6f line contains a tet-off system, by which transgene

expression can be suppressed upon doxycycline treatment ((Garner et al., 2012; Gossen and Bujard, 1992). However, doxycycline treatment is not necessary in these animals, since the Rasgrf2-2A-dCre line holds an inducible system of its own, given that the destabilized Cre (dCre) expressed under the control of the Rasgrf2-2A promoter needs to be stabilized by trimethoprim (TMP) to be fully functional. TMP (Sigma T7883) was reconstituted in Dimethyl sulfoxide (DMSO, Sigma 34869) at a saturation level of 100 mg/ml, freshly prepared for each experiment. For TMP induction, mice were given a single intraperitoneal injection (150 µg TMP/g body weight; 29 g needle; 3–5 days post-surgery), diluted in 0.9% saline solution. We used an intact skull preparation (Silasi et al., 2016) for chronic wide-field calcium imaging of neocortical activity(Gilad et al., 2018b). Mice were anesthetized with 2% isoflurane (in pure O2) and body temperature was maintained at 37 °C. We applied local analgesia (lidocaine 1%), exposed and cleaned the skull, and removed some muscles to access the entire dorsal surface of the left hemisphere (Fig. 2a; ~6 × 8 mm2 from ~3 mm anterior to bregma to ~1 mm posterior to lambda; from the midline to at least 5 mm laterally). We built a wall around the hemisphere with adhesive material (iBond; UV-cured) and dental cement "worms" (Charisma). Then, we applied transparent dental cement homogenously over the imaging field (Tetric EvoFlow T1). Finally, a metal post for head fixation was glued on the back of the right hemisphere. This minimally invasive preparation enabled high-quality chronic imaging with high success rate.

Texture discrimination task.

Mice were trained on a go/no-go discrimination task (Fig. 1a) using a data acquisition interface (USB-6008; National Instruments) and custom-written LabVIEW software (National Instruments). Each trial started with an auditory cue (stimulus cue; 2 beeps at 2 kHz, 100-ms duration with 50-ms interval), signaling the approach of either two types of sandpapers (grit size P100: rough texture; P1200: smooth texture; 3M) to the mouse's whiskers as 'go' or 'no-go' textures (Fig. 1a; pseudo-randomly presented with no more than three repetitions). Sandpapers were mounted onto panels attached to a stepper motor (T-NM17A04; Zaber) mounted onto a motorized linear stage (T-LSM100A; Zaber) to move textures in and out of reach of whiskers. The texture stayed in touch with the whiskers for 2 s, and then it was moved out after which an additional auditory cue (response cue; 4 beeps at 4 kHz, 50-ms duration with 25-ms interval)

signaled the start of a 2-s response period. The stimulus and response cues were identical in both textures. The interval between the trails was 6 s (8 s from response to next cue). A water reward (~3 µL) was given to the mouse for licking for the go texture only after the response cue ('Hit'), i.e. for the first correct lick during the response period (Fig. 1a; lick were detected using a piezo sensor). Punishment with white noise was given for licking for the no-go texture ('false alarms'; FA). Licking before the response cue was neither rewarded nor punished. Reward and punishment were omitted when mice withheld licking for the no-go ('correct-rejections', CR) or go ('Misses') textures.

Training and performance. Five mice were trained to lick for the P100 texture (mice #1-4 and 6) and 2 mice were trained to lick for the P1200 texture (mice #5 and 7). Mice were first handled and accustomed to head fixation before starting water scheduling. Before imaging began mice were conditioned to lick for reward after the go texture (presented within a similar trial structure as the task itself). Imaging began only after mice reliably licked for the response cue (typically after the first day; 200–400 trials). On the first day of imaging, mice were presented with the 'go' texture and after 50 trials the 'no-go' texture was gradually introduced (starting from 10% and increasing by 10% approximately every 50 trials (Guo et al., 2014) until reaching 50% probability for the no-go texture by the end of the day. 6 out of the 7 mice learned the task within 3–4 days after around a thousand trials (Supplementary Fig. 1). Mouse #4 learned the task within 10 days. An effort was made to maintain a constant position of the texture and cameras across imaging days in order to maintain similar stimulation and imaging parameters.

Wide-field calcium imaging. We used a wide-field approach to image large parts of the dorsal cortex while mice learned to perform the task (Gilad et al., 2018b) .A sensitive CMOS camera (Hamamatsu Orca Flash 4.0) was mounted on top of a dual objective setup. Two objectives (Navitar; top objective: D-5095, 50 mm f0.95; bottom objective inverted: D-2595, 25 mm f0.95) were interfaced with a dichroic (510 nm; AHF; Beamsplitter T510LPXRXT) filter cube (Thorlabs). This combination allowed a ~9-mm field-of-view, covering most of the dorsal cortex of the hemisphere contralateral to texture presentation. Blue LED light (Thorlabs; M470L3) was guided through an excitation filter (480/40 nm BrightLine HC), a diffuser, collimated, reflected from the dichroic mirror, and focused through the bottom objective ~100 µm below the blood vessels. Green light emitted from the preparation passed through both objectives and

an emission filter (514/30 nm BrightLine HC) before reaching the camera. The total power of blue light on the preparation was <5mW; i.e., <0.1 mW/mm2. At this illumination power we did not observe any photobleaching. Data was collected with a temporal resolution of 20 Hz and a spatial sampling of 512 × 512 pixels, resulting in a spatial resolution of ~20 µm/pixel. On each imaging day a green reflectance image was taken as reference to enable registration across different imaging days using the blood vessel pattern (fibercoupled LED illuminated from the side; Thorlabs).

Mapping and area selection. Each mouse underwent a mapping session under anesthesia (1% isoflurane), in which we presented five different sensory stimuli (contra-lateral side (Gilad and Helmchen, 2020). Next, we registered each imaging day to the mapping day using skull coordinates from the green images. Finally, we registered each mouse onto a 2D top view mouse atlas using both functional patches from the mapping and skull coordinates ((Gilad and Helmchen, 2020);©2004 Allen Institute for Brain Science. Allen Mouse Brain Atlas. Available from: http://mouse.brain-map.org/29). Within the atlas borders, we defined 25 areas of interest, with some manual modifications within these borders to fit the functional activity for each mouse. Motor cortex areas were defined based on stereotaxic coordinates and functional patches for each mouse (see below). Thus, all mice had similar regions of interest that were comparable within and across mice. We grouped these 25 areas into auditory (green), association (pink), somatosensory + V1 (blue), and motor (red) areas (Fig. 1d and Supplementary Fig. 1b). Auditory areas: Primary auditory (A1), Auditory dorsal (AD) and Temporal association area (TEA). Sensory areas: Somatosensory mouth (Mo), Somatosensory nose (No), Somtosensory hindlimb (HL), Somtosensory forelimb (FL), Barrel cortex (BC; Primary somatosensory whisker); Secondary somatosensory whisker (S2), Somtosensory trunk (Tr) and Primary visual cortex (V1). Motor areas: whisker-related primary motor cortex (M1; 1.5 anterior and 1mm lateral from bregma, corresponding to the whisker evoked activation patch in M1 from the mapping session), anterior lateral motor cortex (ALM; 2.5 anterior and 1.5 mm lateral from bregma69) and secondary motor cortex (M2; 1.5 anterior and 0.5mm lateral from bregma corresponding11). Association cortex: Rostrolateral (RL), Anterior (A), Anterior lateral (AL), Anterior medial (AM), Posterior medial (PM), Lateral medial (LM), Lateral intermediate (LI), Posterior lateral (PL), Post-rhinal (PR), Retrosplenial dorsal (RD) and Retrosplenial angular (RA). We note that our definition of association

cortex is broad and may include or exclude areas that are not necessarily classical association areas.

Whisker and body tracking. In addition to wide-field imaging, we tracked movements of the whiskers and the body of the mouse during the task (Fig. 1a). The mouse was illuminated with a 940-nm infrared LED. Whiskers were imaged at 50 Hz (500 × 500 pixels) using a high-speed CMOS camera (A504k; Basler), from which we calculated time course of whisking envelope and the time of first touch (see below). An additional camera monitored the movements of the mouse at 30 Hz (The imaging source; DMK 22BUC03; 720 × 480 pixels). We used movements of both forelimbs and the head/neck region to assess body movements, to reliably detect large movements (Fig. 1a; see Data Analysis below).

Calculating body movements. We used a body camera to detect general movements of the mouse (30 Hz frame rate). For each imaging day, we first outlined the forelimbs and the neck areas (one area of interest for each), which were reliable areas to detect general movements. Next, we calculated the body movement (1 minus frame-to-frame correlation) within these areas as a function of time for each trial. We than averaged all the defined body areas to one "body" vector.

Whisker tracking. The average whisker angle across all imaged whiskers was measured using automated whisker tracking software (Knutsen et al., 2004) . The mean whisker envelope was calculated as the difference between maximum and minimum whisker angles along a sliding window equal to the imaging frame duration (50 ms; (Gilad et al., 2018b)). Whisker envelope was normalized just before the auditory cue similar to wide-field data (Frame zero). In addition, we manually detected the first frame, in which any whisker touched the upcoming texture, using the movies from the whisker camera (LabVIEW custom program). The first touch occurred on average 0.33 and 0.34 s before the texture stopped for naïve and expert mice respectively. Time of first touch did not differ between expert and naïve mice ($P > 0.05$; Mann–Whitney U-test; $n = 7$ mice). We note that the first touch occurred mostly (but not exclusively) in the pre-period from −1 to −0.5 relative to texture stop.

Data analysis. Data analysis was performed using Matlab software (Mathworks). All mice were continuously imaged during learning (5–11 days). Wide-field fluorescence images were sampled down to 256 × 256 pixels and pixels outside the imaging area were discarded. This resulted in a spatial resolution of ~40 µm/pixel and was sufficient

to determine cortical borders, despite further scattering of emitted light through the tissue and skull. Each pixel and each trial were normalized to baseline several frames before the stimulus cue (frame 0 division). Our main focus was on the history effect. Because the hit trails had the largest portion from all trails, we focused on the hit trials. We sub grouped all the Hit trials based on the type of the preceding trial as follow: CR-Hit - Hit trials that were preceded by correct rejection trial. Hit-Hit - Hit trials that were preceded by a Hit trial. FA-Hit - hit trials that were preceded by a false alarm trial. We mainly focused on comparing Hit-Hit and CR-Hit pairs since they had a large proportion in naïve, learning and expert phases (but see Figure s4). We defined two time periods within the trial structure: pre (−1 to 0.6 s relative to texture stop) and stim (−0.2 to 0.2 relative to texture stop; Fig. 1a).

Calculation of learning curves. Trials were binned (n = 100 trials with no overlap) across learning (at the stimulus time, adjusted for each mouse) and the performance (defined as d' = Z(Hit/(Hit +Miss)) – Z(FA/(FA + CR)) where Z denotes the inverse of the cumulative distribution function) was calculated for each bin. Next, each behavioral learning curve was fitted with a sigmoid function $s(t) = a\frac{1}{1+e^{-(t-b)/c}}$ Where a denotes the amplitude, b the time point (in trial numbers) of the inflection point, and c the steepness of the sigmoid.

A learning threshold was defined as the bin in which the d' crossed the inflection point (half point) of the learning curve sigmoid fit. (Fig. s1).

Defining the learning phases: We defined the naïve, learning and expert phase each as one day of recordings, the naïve day was defined as the first day to have enough correct rejections that the performance is still before the crossing threshold (typically the 2nd recording day). The learning day was defined as the day that the mouse crossed the learning threshold, and the expert was defined as the last day of the mouse (usually the 5th day)

Calculating history modulation and onset: We defined the 'history modulation' as the difference between the average activation of all CR-Hit and Hit-Hit trials. To calculate significance of history modulation, we calculated the sample distribution by trial shuffling between CR-Hit and Hit-Hit trials (n=1000 iterations). We than defined the onset of the history modulation as the first bin exceeding mean ± 2 SD of the sample

565 distribution. We calculated this history modulation and significance across the trial
566 dimension (every frame) and across learning dimension (every 100 trials). In the
567 learning dimension, we calculated the average activity in the stim period (-0.2:0.2) of
568 all the CR-Hit and Hit-Hit trials that were falling within each 100 trials bin.

569 **Discrimination power between hit trials sub grouped by history**. To measure how well
570 could neuronal populations discriminate between go and no-go textures, we calculated
571 a receiver operating characteristics (ROC) curve and calculated its area under the curve
572 (AUC; with a value of 0.5 indicating no discrimination power). This can be done for a
573 given area, each time frame within each learning phase separately (Fig. 6).
574
575 **Statistical analysis**. In general, the Wilcoxon signed-rank test to compare a
576 population's median to zero (or between two paired populations). Multiple group
577 correction was used when comparing between more than two groups.
578

579 **References:**

580

581 Akrami A, Kopec CD, Diamond ME, Brody CD. 2018. Posterior parietal cortex
582 represents sensory history and mediates its effects on behaviour. *Nature*
583 **554**:368–372. doi:10.1038/nature25510

584 Banerjee A, Parente G, Teutsch J, Lewis C, Voigt FF, Helmchen F. 2020. Value-guided
585 remapping of sensory cortex by lateral orbitofrontal cortex. *Nature* **585**:245–
586 250. doi:10.1038/S41586-020-2704-Z

587 Blake DT, Strata F, Churchland AK, Merzenich MM. 2002. Neural correlates of
588 instrumental learning in primary auditory cortex. *Proc Natl Acad Sci U S A*
589 **99**:10114–10119. doi:10.1073/pnas.092278099

590 Chen JL, Carta S, Soldado-Magraner J, Schneider BL, Helmchen F. 2013. Behaviour-
591 dependent recruitment of long-range projection neurons in somatosensory
592 cortex. *Nature* **499**:336–340. doi:10.1038/nature12236

593 Chen JL, Margolis DJ, Stankov A, Sumanovski LT, Schneider BL, Helmchen F. 2015.
594 Pathway-specific reorganization of projection neurons in somatosensory cortex
595 during learning. *Nat Neurosci* **18**:1101–1108. doi:10.1038/nn.4046

596 Chéreau R, Bawa T, Fodoulian L, Carleton A, Pagès S, Holtmaat A. 2020. Dynamic
597 perceptual feature selectivity in primary somatosensory cortex upon reversal
598 learning. *Nat Commun* **11**. doi:10.1038/s41467-020-17005-x

599 Driscoll LN, Pettit NL, Minderer M, Chettih SN, Harvey CD. 2017a. Dynamic
600 Reorganization of Neuronal Activity Patterns in Parietal Cortex. *Cell* **170**:986–
601 999.e16. doi:10.1016/j.cell.2017.07.021

602 Driscoll LN, Pettit NL, Minderer M, Chettih SN, Harvey CD, Driscoll LN, Pettit NL,
603 Minderer M, Chettih SN, Harvey CD. 2017b. Dynamic Reorganization of
604 Neuronal Activity Patterns in Parietal Cortex Article Dynamic Reorganization of
605 Neuronal Activity Patterns in Parietal Cortex. *Cell* **170**:1–14.
606 doi:10.1016/j.cell.2017.07.021

607 Estebanez L, Boustani S el, Destexhe A, Shulz DE. 2012. Correlated input reveals
608 coexisting coding schemes in a sensory cortex. *Nat Neurosci* **15**:1691–1699.
609 doi:10.1038/nn.3258

610 Fu Y, Kaneko M, Tang Y, Alvarez-Buylla A, Stryker MP. n.d. A cortical disinhibitory
611 circuit for enhancing adult plasticity. doi:10.7554/eLife.05558.001

612 Gallero-Salas Y, Han S, Sych Y, Voigt FF, Laurenczy B, Gilad A, Helmchen F. 2021.
613 Sensory and Behavioral Components of Neocortical Signal Flow in
614 Discrimination Tasks with Short-Term Memory. *Neuron* **109**:135–148.e6.
615 doi:10.1016/J.NEURON.2020.10.017

616 Garion L, Dubin U, Rubin Y, Khateb M, Schiller Y, Azouz R, Schiller J. 2014. Texture
617 coarseness responsive neurons and their mapping in layer 2-3 of the rat barrel
618 cortex in vivo. *Elife* **3**:e03405. doi:10.7554/ELIFE.03405

Garner AR, Rowland DC, Hwang SY, Baumgaertel K, Roth BL, Kentros C, Mayford M. 2012. Generation of a Synthetic Memory Trace. *Science (1979)* **335**:1513–1516. doi:10.1126/science.1214985

Garrett M, Manavi S, Roll K, Ollerenshaw DR, Groblewski PA, Ponvert ND, Kiggins JT, Casal L, Mace K, Williford A, Leon A, Jia X, Ledochowitsch P, Buice MA, Wakeman W, Mihalas S, Olsen SR. 2020. Experience shapes activity dynamics and stimulus coding of VIP inhibitory cells. *Elife* **9**. doi:10.7554/eLife.50340

Gilad A, Gallero-Salas Y, Groos D, Helmchen F. 2018a. Behavioral Strategy Determines Frontal or Posterior Location of Short-Term Memory in Neocortex. *Neuron* **99**:814–828.e7. doi:10.1016/j.neuron.2018.07.029

Gilad A, Gallero-salas Y, Groos D, Helmchen F, Gilad A, Gallero-salas Y, Groos D, Helmchen F. 2018b. Behavioral Strategy Determines Frontal or Posterior Location of Short-Term Memory in Neocortex. *Neuron* **99**:814–828.e7. doi:10.1016/j.neuron.2018.07.029

Gilad A, Helmchen F. 2020. Spatiotemporal refinement of signal flow through association cortex during learning. *Nat Commun* **11**:1–14. doi:10.1038/s41467-020-15534-z

Gilad A, Maor I, Mizrahi A. 2020. Learning-related population dynamics in the auditory thalamus. *Elife* **9**:1–18. doi:10.7554/eLife.56307

Gilad A, Meirovithz E, Slovin H. 2013. Population Responses to Contour Integration: Early Encoding of Discrete Elements and Late Perceptual Grouping. *Neuron* **78**:389–402. doi:10.1016/j.neuron.2013.02.013

Gossen M, Bujard H. 1992. Tight control of gene expression in mammalian cells by tetracycline-responsive promoters. *Proc Natl Acad Sci U S A* **89**:5547–5551. doi:10.1073/pnas.89.12.5547

Guo Z, Li N, Huber D, Ophir E, Gutnisky D, Ting J, Feng G, Svoboda K. 2014. Flow of cortical activity underlying a tactile decision in mice. *Neuron* **81**:179–194. doi:10.1016/j.neuron.2013.10.020

Harvey CD, Coen P, Tank DW. 2012. Choice-specific sequences in parietal cortex during a virtual-navigation decision task. *Nature* **484**:62–68. doi:10.1038/nature10918

Hattori R, Danskin B, Babic Z, Mlynaryk N, Komiyama T. 2019. Area-Specificity and Plasticity of History-Dependent Value Coding During Learning. *Cell* **177**:1858–1872.e15. doi:10.1016/j.cell.2019.04.027

Hovde K, Gianatti M, Witter MP, Whitlock JR. 2018. Architecture and organization of mouse posterior parietal cortex relative to extrastriate areas. *European Journal of Neuroscience* **49**:1313–1329. doi:10.1111/ejn.14280

Hwang EJ, Dahlen JE, Mukundan M, Komiyama T. 2017. History-based action selection bias in posterior parietal cortex. *Nat Commun* **8**:1–14. doi:10.1038/s41467-017-01356-z

Johnson CM, Peckler H, Tai LH, Wilbrecht L. 2016. Rule learning enhances structural plasticity of long-range axons in frontal cortex. *Nature Communications 2016 7:1* **7**:1–14. doi:10.1038/ncomms10785

Jurjut O, Georgieva P, Busse L, Katzner S. 2017. Learning Enhances Sensory Processing in Mouse V1 before Improving Behavior. *J Neurosci* **37**:6460–6474. doi:10.1523/JNEUROSCI.3485-16.2017

Kawai T, Yamada H, Sato N, Takada M, Matsumoto M. 2015. Roles of the Lateral Habenula and Anterior Cingulate Cortex in Negative Outcome Monitoring and Behavioral Adjustment in Nonhuman Primates. *Neuron* **88**:792–804. doi:10.1016/J.NEURON.2015.09.030

Khodagholy D, Gelinas JN, Buzsáki G. 2017. Learning-enhanced coupling between ripple oscillations in association cortices and hippocampus. *Science* **358**:369–372. doi:10.1126/science.aan6203

Khodagholy D, Gelinas JN, Buzsáki G. n.d. Learning-enhanced coupling between ripple oscillations in association cortices and hippocampus.

Knutsen PM, Derdikman D, Ahissar E. 2004. Tracking Whisker and Head Movements in Unrestrained Behaving Rodents. *J Neurophysiol* **93**:2294–2301. doi:10.1152/jn.00718.2004

Komiyama T, Sato TR, O'Connor DH, Zhang Y-X, Huber D, Hooks BM, Gabitto M, Svoboda K. 2010. Learning-related fine-scale specificity imaged in motor cortex circuits of behaving mice. *Nature* **464**:1182–1186. doi:10.1038/nature08897

Lacefield CO, Pnevmatikakis EA, Paninski L, Bruno RM. 2019. Reinforcement Learning Recruits Somata and Apical Dendrites across Layers of Primary Sensory Cortex. *Cell Rep* **26**:2000-2008.e2. doi:10.1016/j.celrep.2019.01.093

le Merre P, Esmaeili V, Charrière E, Galan K, Salin PA, Petersen CCH, Crochet S. 2018. Reward-Based Learning Drives Rapid Sensory Signals in Medial Prefrontal Cortex and Dorsal Hippocampus Necessary for Goal-Directed Behavior. *Neuron* **97**:83–91.e5. doi:10.1016/j.neuron.2017.11.031

Li W, Piëch V, Gilbert CD. 2008. Learning to link visual contours. *Neuron* **57**:442–451. doi:10.1016/j.neuron.2007.12.011

Lyamzin D, Benucci A. 2019. The mouse posterior parietal cortex: Anatomy and functions. *Neurosci Res* **140**:14–22. doi:10.1016/j.neures.2018.10.008

Marcos AS, Harvey CD. 2016. History-dependent variability in population dynamics during evidence accumulation in cortex. *Nat Neurosci* **19**:1672–1680. doi:10.1038/nn.4403

Mohan H, An X, Kondo H, Zhao S, Matho KS, Musall S, Mitra P, Huang ZJ. 2022. Cortical glutamatergic projection neuron types contribute to distinct functional subnetworks. *bioRxiv* 2021.12.30.474537. doi:10.1101/2021.12.30.474537

Morcos AS, Harvey CD. 2016. History-dependent variability in population dynamics during evidence accumulation in cortex **19**. doi:10.1038/nn.4403

Musall S, Sun XR, Mohan H, An X, Gluf S, Drewes R, Osten P, Churchland AK. n.d. Pyramidal cell types drive functionally distinct cortical activity patterns during decision-making. doi:10.1101/2021.09.27.461599

Oh SW, Harris JA, Ng L, Winslow B, Cain N, Mihalas S, Wang Q, Lau C, Kuan L, Henry AM, Mortrud MT, Ouellette B, Nguyen TN, Sorensen SA, Slaughterbeck CR, Wakeman W, Li Y, Feng D, Ho A, Nicholas E, Hirokawa KE, Bohn P, Joines KM, Peng H, Hawrylycz MJ, Phillips JW, Hohmann JG, Wohnoutka P, Gerfen CR, Koch C, Bernard A, Dang C, Jones AR, Zeng H. 2014. A mesoscale connectome of the mouse brain. *Nature* **508**:207–214. doi:10.1038/nature13186

Pasupathy A, Miller EK. 2005. Different time courses of learning-related activity in the prefrontal cortex and striatum **1138**:873–876.

Petreanu L, Gutnisky DA, Huber D, Xu NL, Oconnor DH, Tian L, Looger L, Svoboda K. 2012. Activity in motor–sensory projections reveals distributed coding in somatosensation. *Nature 2012 489:7415* **489**:299–303. doi:10.1038/nature11321

Pfeffer CK, Xue M, He M, Huang ZJ, Scanziani M. 2013. Inhibition of inhibition in visual cortex: The logic of connections between molecularly distinct interneurons. *Nat Neurosci* **16**:1068–1076. doi:10.1038/nn.3446

Pho GN, Goard MJ, Woodson J, Crawford B, Sur M. 2018. Task-dependent representations of stimulus and choice in mouse parietal cortex. *Nat Commun* **9**. doi:10.1038/s41467-018-05012-y

Poort J, Khan AG, Pachitariu M, Nemri A, Orsolic I, Krupic J, Bauza M, Sahani M, Keller GB, Mrsic-Flogel TD, Hofer SB. 2015. Learning Enhances Sensory and Multiple Non-sensory Representations in Primary Visual Cortex. *Neuron* **86**:1478–1490. doi:10.1016/j.neuron.2015.05.037

Rodgers CC, Nogueira R, Pil BC, Greeman EA, Park JM, Hong YK, Fusi S, Bruno RM. 2021. Sensorimotor strategies and neuronal representations for shape discrimination. *Neuron* **109**:2308-2325.e10. doi:10.1016/j.neuron.2021.05.019

Roelfsema PR, Holtmaat A. 2018. Control of synaptic plasticity in deep cortical networks. *Nat Rev Neurosci*. doi:10.1038/nrn.2018.6

Safaai H, von Heimendahl M, Sorando JM, Diamond ME, Maravall M. 2013. Coordinated Population Activity Underlying Texture Discrimination in Rat Barrel Cortex. *Journal of Neuroscience* **33**:5843–5855. doi:10.1523/JNEUROSCI.3486-12.2013

Save E, Poucet B. 2009. Role of the parietal cortex in long-term representation of spatial information in the rat. *Neurobiol Learn Mem* **91**:172–178. doi:10.1016/j.nlm.2008.08.005

Scott Benjamin B, Constantinople CM, Akrami A, Hanks TD, Brody CD, Tank DW. 2017. Fronto-parietal Cortical Circuits Encode Accumulated Evidence with a Diversity of Timescales. *Neuron* **95**:385–398.e5. doi:10.1016/j.neuron.2017.06.013

Scott Benjamin B., Constantinople CM, Akrami A, Hanks TD, Brody CD, Tank DW. 2017. Fronto-parietal Cortical Circuits Encode Accumulated Evidence with a Diversity of Timescales. *Neuron* **95**:385-398.e5. doi:10.1016/J.NEURON.2017.06.013

Silasi G, Xiao D, Vanni MP, Chen ACN, Murphy TH. 2016. Intact skull chronic windows for mesoscopic wide-field imaging in awake mice. *J Neurosci Methods* **267**:141–149. doi:10.1016/j.jneumeth.2016.04.012

Sul JH, Kim H, Huh N, Lee D, Jung MW. 2010. Distinct Roles of Rodent Orbitofrontal and Medial Prefrontal Cortex in Decision Making. *Neuron* **66**:449–460. doi:10.1016/J.NEURON.2010.03.033

Suzuki A, Kosugi S, Murayama E, Sasakawa E, Ohkawa N, Konno A, Hirai H, Inokuchi K. 2022. A cortical cell ensemble in the posterior parietal cortex controls past experience-dependent memory updating. *Nat Commun* **13**. doi:10.1038/s41467-021-27763-x

Tsutsui KI, Grabenhorst F, Kobayashi S, Schultz W. 2016. A dynamic code for economic object valuation in prefrontal cortex neurons. *Nature Communications 2016 7:1* **7**:1–16. doi:10.1038/ncomms12554

Vann SD, Aggleton JP, Maguire EA. 2009. What does the retrosplenial cortex do? *Nat Rev Neurosci* **10**:792–802. doi:10.1038/nrn2733

Vanni MP, Murphy TH. 2014. Mesoscale Transcranial Spontaneous Activity Mapping in GCaMP3 Transgenic Mice Reveals Extensive Reciprocal Connections between Areas of Somatomotor Cortex. *Journal of Neuroscience* **34**:15931–15946. doi:10.1523/JNEUROSCI.1818-14.2014

Vecchia D, Beltramo R, Vallone F, Chéreau R, Forli A, Molano-Mazón M, Bawa T, Binini N, Moretti C, Holtmaat A, Panzeri S, Fellin T. 2020. Temporal Sharpening of Sensory Responses by Layer V in the Mouse Primary Somatosensory Cortex. *Current Biology* **30**:1589-1599.e10. doi:10.1016/j.cub.2020.02.004

Whitlock JR, Sutherland RJ, Witter MP, Moser M-B, Moser EI. 2008. Navigating from hippocampus to parietal cortex.

Wiest MC, Thomson E, Pantoja J, Nicolelis MAL. 2010. Changes in S1 Neural Responses During Tactile Discrimination Learning. *J Neurophysiol* **104**:300–312. doi:10.1152/jn.00194.2010

Williams LE, Holtmaat A. 2019. Higher-Order Thalamocortical Inputs Gate Synaptic Long-Term Potentiation via Disinhibition. *Neuron* **101**:91–102.e4. doi:10.1016/j.neuron.2018.10.049

Xu J, Harvey N, Saito T, Fukai A, Mabuchi A, Ikeda T, Yano F, Ohba S, Nishida N, Akune T, Yoshimura N, Nakagawa T, Nakamura K, Tokunaga K, Chung U-I, Kawaguchi H, Makino H, Komiyama T. 2014. Learning enhances the relative impact of top-down processing in the visual cortex. *Cognition* **2015**:173–180. doi:10.1038/nn.4061

779 Yan Y, Rasch MJ, Chen M, Xiang X, Huang M, Wu S, Li W. 2014. Perceptual training
780 continuously refines neuronal population codes in primary visual cortex. *Nat*
781 *Neurosci* **17**:1380–1387. doi:10.1038/nn.3805

782 Zuo Y, Diamond ME. 2019. Texture Identification by Bounded Integration of Sensory
783 Cortical Signals. *Current Biology* **29**:1425-1435.e5.
784 doi:10.1016/j.cub.2019.03.017

785

786

Supplemental information:

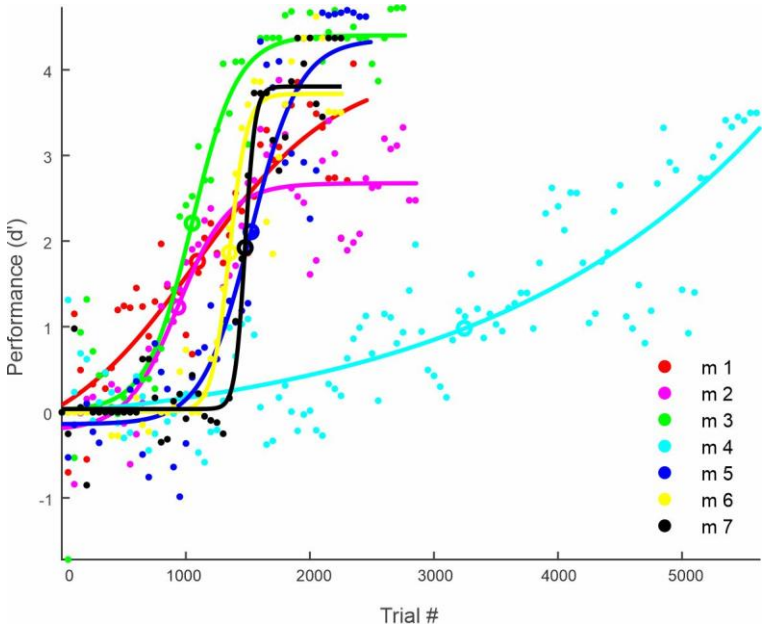

Figure s1. Learning curves of all 7 mice.
Performance (d') for all mice across the entire learning period is calculated for every 50 trails, fitted with a sigmoid function. The inflection point of the sigmoid fit is defined as the learning threshold and indicated by open circle for each mouse.

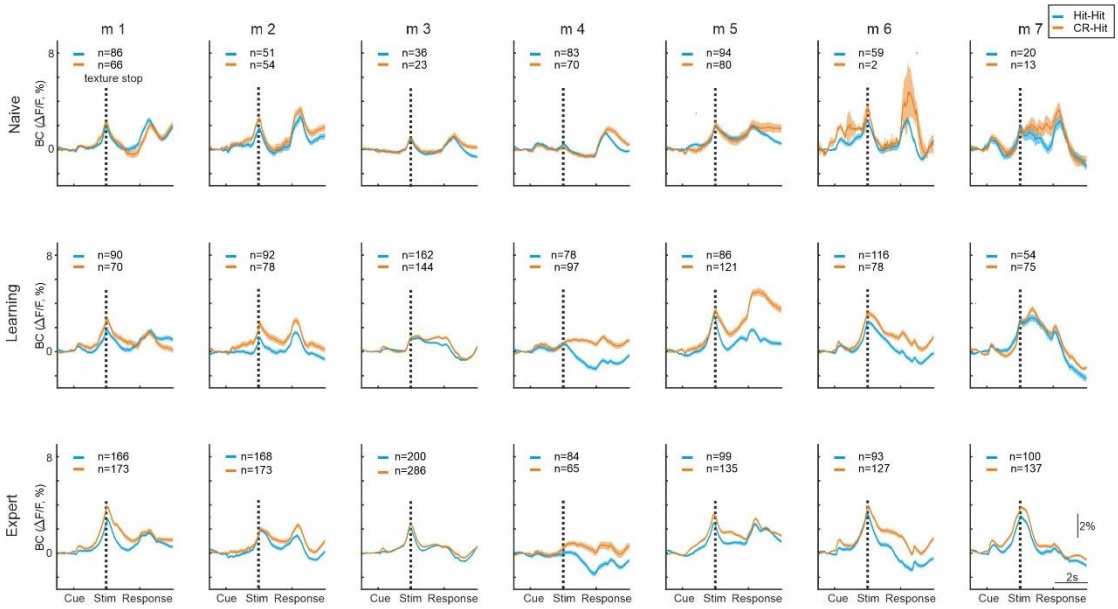

Figure s2. Time course of each mouse in the naïve, learning and expert phase for hit trials classified by preceding trial.

Vertical dashed line denote texture stop. Shadows are mean±SEM across trials

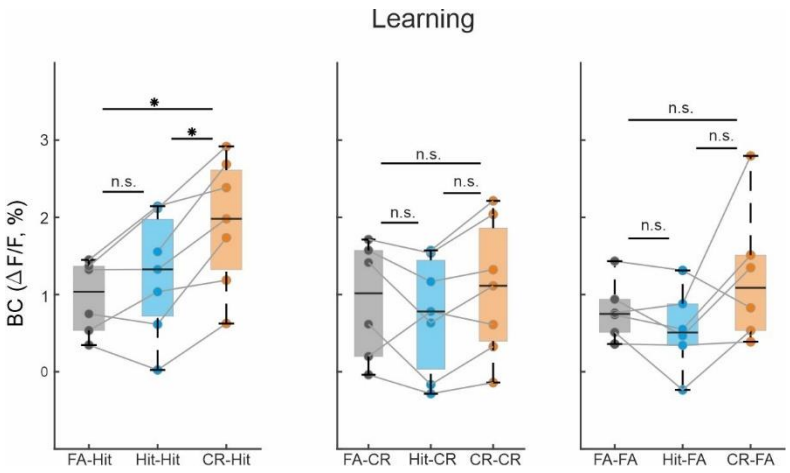

Figure s3. Correct rejection trials have the strongest history effect.

Grand average of BC activity of all history combinations in the learning phase during the stim period (-0.2–0.6ms). Boxes indicate quartiles at 25/75th percentile across mice (n=7). *p < 0.05; n.s. not significant; Wilcoxon signed-rank test.

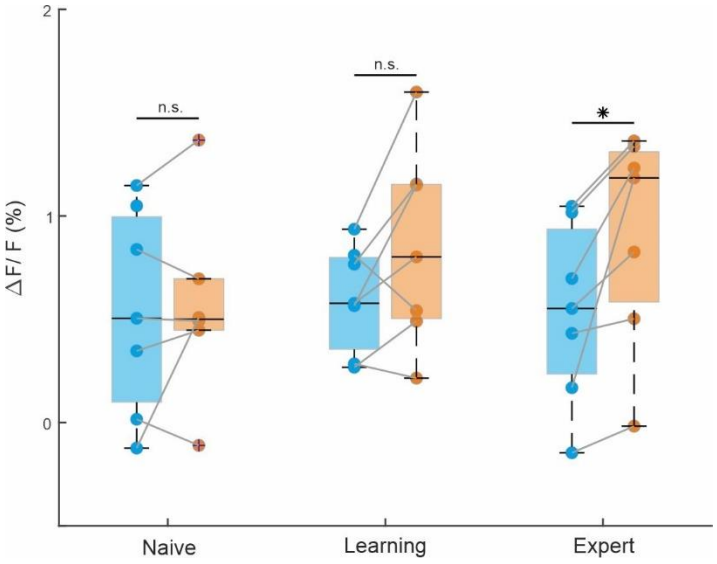

Figure s4. RL activity at pre-stim period (-1– -0.6) across learning.

Boxes indicate quartiles at 25/75th percentile across mice (n=7). *p < 0.05; n.s. not significant; Wilcoxon signed-rank test.